Eur. Phys. J. E (2011) **34**: 49
DOI 10.1140/epje/i2011-11049-0

THE EUROPEAN PHYSICAL JOURNAL E

Regular Article

# Nonlinear ionic pulses along microtubules

D.L. Sekulić[1,a], B.M. Satarić[1], J.A. Tuszynski[2,3], and M.V. Satarić[1]

[1] Faculty of Technical Sciences, University of Novi Sad, Trg D. Obradovića 6, 21000 Novi Sad, Serbia
[2] Department of Oncology, Cross Cancer Institute, University of Alberta, Edmonton, Alberta, Canada
[3] Department of Physics, University of Alberta, Edmonton, Alberta, Canada

Received 27 December 2010 and Received in final form 24 March 2011
Published online: 23 May 2011 – 

**Abstract.** Microtubules are cylindrically shaped cytoskeletal biopolymers that are essential for cell motility, cell division and intracellular trafficking. Here, we investigate their polyelectrolyte character that plays a very important role in ionic transport throughout the intra-cellular environment. The model we propose demonstrates an essentially nonlinear behavior of ionic currents which are guided by microtubules. These features are primarily due to the dynamics of tubulin C-terminal tails which are extended out of the surface of the microtubule cylinder. We also demonstrate that the origin of nonlinearity stems from the nonlinear capacitance of each tubulin dimer. This brings about conditions required for the creation and propagation of solitonic ionic waves along the microtubule axis. We conclude that a microtubule plays the role of a biological nonlinear transmission line for ionic currents. These currents might be of particular significance in cell division and possibly also in cognitive processes taking place in nerve cells.

## 1 Introduction

Microtubules (MTs) are major cytoskeletal protein polymers assembled from the protein called tubulin that plays a number of crucial biological roles in all eukaryotic cells [1]. The role of MTs in cell division has been extensively discussed in the cell biology literature. In this paper, we focus on the importance of MTs in the process of ionic current regulation within biological cells. Many years ago Matsumoto *et al.* [2] revealed that axoplasmic MTs and 260 K proteins in the structure underlying the axolema play a role in generating $Na^+$ currents in squid giant axons. Another seminar paper [3] considered the importance of $Ca^{++}$ ionic currents in cell division and emphasized that MTs in the mitotic apparatus might be controlled by the local $Ca^{++}$ concentration which should be tuned by nearby endoplasmic reticulum (ER). Spindle MTs appear to be very sensitive to $Ca^{++}$ concentration increases in such a way that MT depolymerisation occurs when the concentration is raised above 1 $\mu$M. It was suggested that during anaphase $Ca^{++}$ release from ER activates MT depolymerisation and this facilitates movement of chromosomes to the spindle poles [4]. Here, we postulate that localized $Ca^{++}$ ionic currents along MTs serve as triggers for the onset of their depolymerisation. The synchronously regulated separation of sister chromatid pairs in mitotic spindles has been recently described by Matsson [5,6] using an elegant nonlinear theoretical model. We propose that the process of MT depolymerisation involved in cell division is finely orchestrated by $Ca^{++}$ influx from ER which propagates along MTs as a nonlinear wave.

The structure of MTs is cylindrical and it typically involves 13 parallel protofilaments *in vivo*, see fig. 1. The building block of a MT is a tubulin dimer (TD) that contains approximately 900 amino acid residues comprising some 14000 atoms with a combined mass of 110 kDa (1 Da is the atomic unit of mass, 1 Da = $1.7 \times 10^{-27}$ kg). The TD is made up of two structurally slightly different monomers called $\alpha$ and $\beta$ tubulin, respectively. Each TD in the MT has a length of 8 nm along the MT cylinder axis, a width of about 6.5 nm and the radial dimension of 4.6 nm. The inner core of the cylinder, known as the lumen, is approximately 15 nm in diameter. The surface of MTs is mostly characterized by a so-called B-lattice structure [7], see fig. 2.

Between neighboring protofilaments there are two distinct types of nanopores (NP). NP-1, see fig. 2, left panel, is located where an inter-dimer $\beta/\alpha$ interface of one TD lies next to the inter-dimer $\beta/\alpha$ interface of the adjacent TD molecule. The so-called NP-2 arises where an intra-dimer interface of one dimer lies next to the intra-dimer interface of an adjacent TD of a neighboring protofilament, see fig. 2, right panel. Freedman *et al.* [8] used HOLE and AMBER programs to estimate the effective radius of the narrowest points within these NPs and found them to be 0.4 nm and 0.47 nm for type-1 and type-2 NPs, respectively.

The biological relevance of NPs in MT is still largely unknown. However, it has been experimentally determined

[a] e-mail: dalsek@yahoo.com

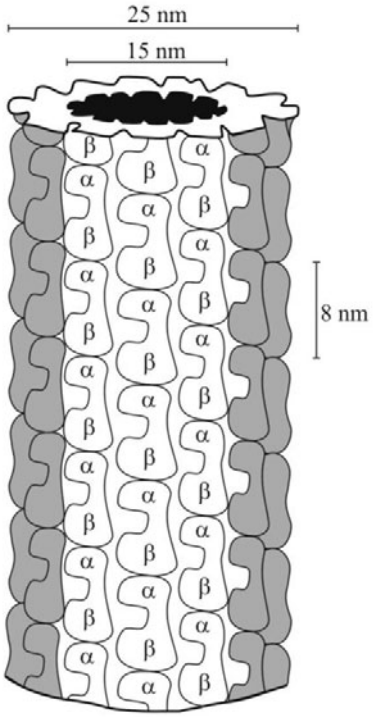


**Fig. 1.** A MT hollow cylinder of 13 parallel protofilaments with denoted characteristic dimensions: outer and inner diameters of 25 nm and 15 nm, respectively, and tubulin dimer length of 8 nm.

that the molecules of some chemotherapy drugs such as paclitaxel and epothilone diffuse through MT NPs to their corresponding binding sites mostly positioned in the lumen [9]. Thus, it can be safely assumed that these NPs, on the basis of their size, should be quite permeable to the counter-ions from the ionic clouds covering outer and inner sides of the MT wall. This paper will theoretically examine the role of these NPs in the regulation of ionic currents along MTs within the regime comparable to transmission lines used in electric engineering applications. We have earlier made preliminary attempts to evaluate MTs as nonlinear transmission lines. The first stage was a model which disregards the role of NPs but includes the nonlinear electric capacity of MTs [10]. The outcome of this model was the appearance of stable localized kink-like pulses of cations propagating along MTs. The next step was extended by the inclusion of NPs [11]. This approach was based on the simple conical geometry pattern of NPs considered earlier by the group of Eisenberg [12]. This preliminary description of NPs in our model has led to the emergence and propagation of ionic pulses analogous to the celebrated Korteveg de Vries (KdV) solitons and was arrived at using reasonable values of model parameters.

This paper is intended to develop a much more realistic model based on the sophisticated simulations performed by Freedman *et al.* [8]. We briefly state the main results of the simulations reported in [8] which are relevant for the model considered here. Based on the modified version of the Poisson-Boltzmann equation, the conductances of NPs are determined in terms of Brownian dynamics of ions. For the type-1 NP, inner and outer cationic conductances were calculated to be 2.93 nS and 1.22 nS, respectively, while for type-2 NP the respective values of 7.80 nS and 4.98 nS were found. Interestingly, it was demonstrated that both types of NPs are impermeable to anions whose respective conductances are 0.044 nS and 0.012 nS for type-1 and type-2 NPs. Freedman *et al.* [8] also explained in great detail how the constriction zones of NPs, due to the presence of negative ASP and THR residues, prevent the passage of more negative ions through the NPs. Similar asymmetric conductance has been found in various experiments involving ion channels, for example Omp F porin [13].

We now focus on the second, an even more important constituent of MTs in the context of the present model. Each tubulin monomer of the MT lattice has a short C-terminal alpha-helix H12 followed by a highly acidic amino acid sequence projecting out of the MT outer surface which is referred to as a tubulin tail (TT). Geometrically, these TTs are hair-like projections of 4–5 nm length, see fig. 3. Their approximate molecular masses are 5.5 kDa and 6.7 kDa for $\alpha$ and $\beta$ tubulin, respectively. TTs are of great functional importance because they participate in the binding of proteins through which MT interact with many cellular structures such as motor proteins (kinesin and dynein) and a plethora of microtubule associated proteins (MAPs) [14]. Satarić and Tuszynski [15] developed a model of nonlinear waves created by tilting excitations of TTs emphasizing their possible role in the control of motor protein traffic along MTs. In $\alpha$ tubulin the TT consists of the last 10 residues in their sequence, while in $\beta$ tubulin the corresponding TT is longer comprising 18 residues. The most common isotype of $\alpha$ tubulin has a TT with 5 Glu and 2 Asp residues, while its $\beta$ counterpart has 9 Glu and 2 Asp residues. The negative charge on TTs is the reason why they are surrounded by a large number of cations required for overall charge neutrality. The important aspect of the aforementioned modeling [8] is the claim that TTs could contribute to ionic currents flowing along MTs by playing the role of small voltage generators (batteries). This claim is based on their larger time-scale thermal fluctuations which result in an oscillatory transfer of ions between the bulk solution and the cloud of counterions located near the MT surface. Here, we partly rely on the results of the simulations reported in [8] and partly on our earlier transmission line analysis [11], in order to elucidate the possible active role MTs play in ionic signaling throughout cytoskeletal networks.

The paper is organized as follows: In sect. 2 we explain the polyelectrolyte character of MTs. In sect. 3 we describe the basic elements of MTs as a biological nanoscale transmission line. In sect. 4 we analyze a nonlinear differential equation of the modified KdV type for the electric potential accompanying a localized ionic wave along an MT. Then, we solve and analyze the pertaining differential equation which exhibits the common features with spherical and cylindrical solitons arising in ion-acoustic waves in plasma. Section 5 provides conclusions stemming from the results of this paper.

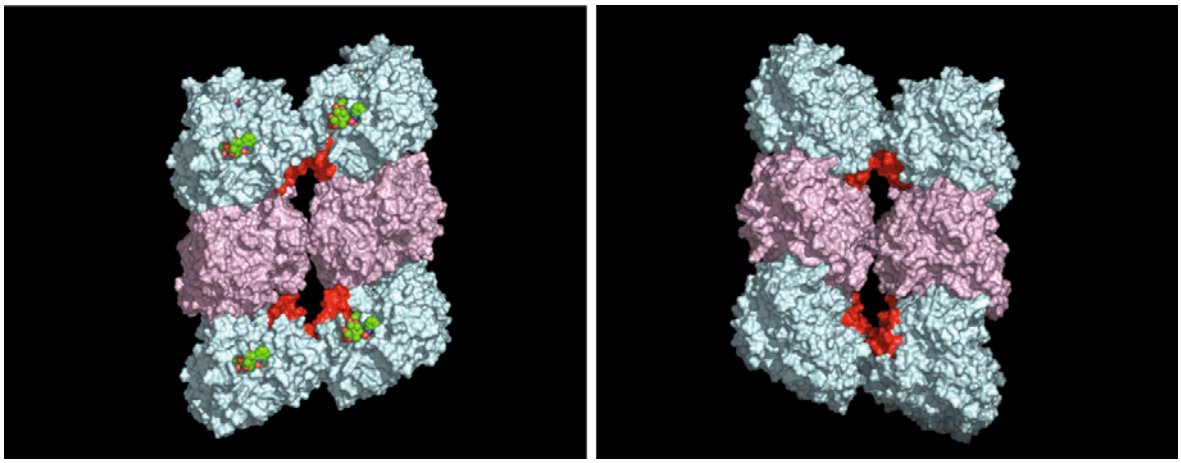

**Fig. 2.** An illustration of the nanopores in the A and B MT lattices, respectively.

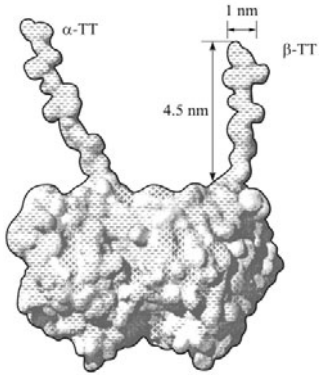


**Fig. 3.** The topology of a tubulin dimer with TTs whose dimensions are: length of 4.5 nm and diameter of 1 nm. The surface charge distribution is indicated by plus and minus signs.

## 2 The biophysical basis for the model

Extensive molecular dynamics simulations were performed on the TD structure and MTs [16,17]. Their results indicate the existence of a highly negatively charged solvent exposed surface of the TD with a net electric charge on the order of (20–25)$e$ per monomer, depending on the isotype of tubulin considered. This net charge is distributed preferentially on the outer surface of the MT at an approximate charge ratio of 2:1 between the outer surface and the rest of the protein. Therefore, we conclude that MTs as highly charged polyelectrolytes are expected to attract a fraction of their surrounding counter-ions in the form of a condensed ionic cloud (IC) preferentially localized around the MT surface.

Manning's theory of polyelectrolyte solutions [18] states that ionic condensation occurs along the stretch of a charged polymer, if a sufficiently high linear electric charge density is present on the polymer's surface. On this basis, it can be concluded that the cylindrical sheath of depleted ions outside the ionic cloud surrounding the MT serves as an electrical shield. The "cable-like" behavior of such a structure can be supported by the protein polymer itself and the "condensed" counter-ions, which are physically "bound" to the polymer. The strength of this interaction has been estimated to be such that even under infinite dilution conditions, the counter-ions are still attached to the polymer and do not diffuse out from its vicinity. Although this theory was originally postulated for such polyelectrolytes as DNA, the same applies to highly charged quasi-one-dimensional, or cylindrical polymers such as actin filaments and MTs. These two cases were studied theoretically in more detail in other publications [8,10,19–22] and we adopt this approximation as valid for the case considered in our paper.

Moreover, experimental confirmation of the novel nonlinear amplification of ionic currents by MTs serves as support for this model [23]. Since our model is directly based on the ionic condensation effect around the MT cylinder, we first evaluate the effective charge density around the MT length. The Bjerrum length, denoted $l_B$, describes the distance beyond which thermal fluctuations are stronger than the electrostatic interactions between charges in solution whose dielectric constant is $\varepsilon$. Specifically, the following equation is satisfied:

$$\frac{e^2}{4\pi\varepsilon_0\varepsilon l_B} = k_B T; \quad \varepsilon_0 = 8.85 \times 10^{-12}\,\mathrm{F/m}. \tag{2.1}$$

At a physiological temperature ($T = 310\,\mathrm{K}$), taking the elementary charge as $e = 1.6 \times 10^{-19}\,\mathrm{C}$, Boltzmann's constant as $k_B = 1.38 \times 10^{-23}\,\mathrm{J/K}$ and the relative dielectric permittivity of the cytosol as $\varepsilon = 80$, one readily obtains

$$l_B = 0.67 \times 10^{-9}\,\mathrm{m} = 0.67\,\mathrm{nm}. \tag{2.2}$$

Accordingly, every MT should attract an IC of positive counter-ions close to its surface and along TTs, while negative ions of the cytosol are repelled away from the MT surface so that a roughly cylindrical ionic depletion area around TDs and TTs emerges. The thickness of such a depleted area is approximately equal to the Bjerrum length.

In addition, counter-ion condensation occurs when the mean distance between two charges, $b$, is such that

$$S = \frac{l_B}{b} > 1. \tag{2.3}$$

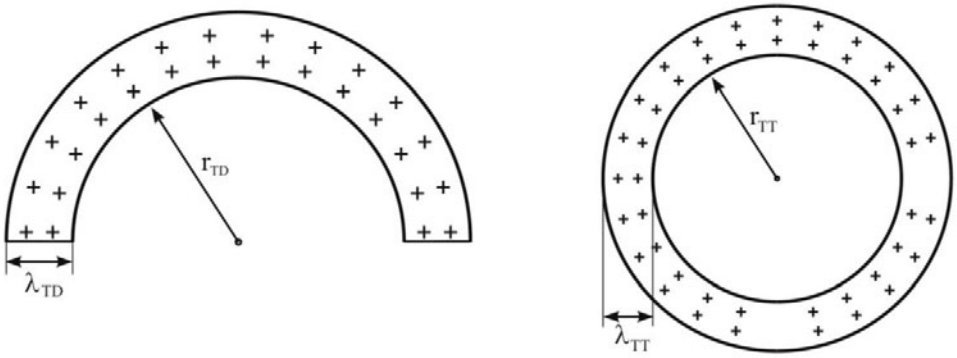


**Fig. 4.** Schematic representation of the counter-ion charge distributions surrounding a microtubule (left panel) and a C-terminal tail (right panel).

As a reasonable approximation we assume that each $\beta$ tubulin monomer carries an excess of 24 negative charges in vacuum while each $\alpha$ tubulin monomer carries 22 charges. Moreover, some 30–40% of the net charge is located in areas of tubulin that are not solvent accessible. Therefore, we expect to have 15–18 exposed negative charges per TD, without counting the charges present on the protruding TTs. Since each dimmer is 8 nm long and 13 protofilaments form a MT, we readily find that there is a linear charge of (20–30)$e$/nm and a linear charge spacing of $b = (0.33\text{–}0.44) \times 10^{-10}$ m which gives $S$ in the range between 16 and 21. As the effective charge $q_{\text{eff}}$ is defined as the bare value of net charge divided by $S$, we estimate it to be $q_{\text{eff}} = (0.43\text{–}0.57)e$/monomer. This quantity has been indirectly measured in experimental assays where MTs were subjected to external electrical fields [23]. However, it should also be noted that this number represents a "far-field" value which could be overly high since it belies additional screening which is achieved by all ions attached to the MT but not all necessarily condensed on it. We conclude that in view of the experimental data, these estimates are acceptable for our continuum model calculations. For this type of model it is important to estimate the thickness of an IC of positive counter-ions around MTs and TTs. This is dictated by the geometry of the surface landscape and by its negative charge distribution.

The occurrence of Manning condensation around the polymer of radius $r$ also depends on the fact that the salt concentration $n$ in the cytosol should be low enough to satisfy the inequality [24]

$$l_{\text{Db}} \gg r, \tag{2.4}$$

where the Debye length $l_{\text{Db}}$ is defined by

$$l_{\text{Db}}^{-1} = (8\pi n l_B)^{1/2}. \tag{2.5}$$

Since the radius of a TT is of the order of 0.5 nm and the radius of a TD is of the order of 2.5 nm, while the Debye length for the cytosol is of the order of 10 nm [25], we see that the condition in (2.4) holds for both radii. Thus, we are now able to reliably estimate the respective condensate thickness $\lambda$

$$\lambda = A(r l_{\text{Db}})^{1/2}; \quad A < 1, \tag{2.6}$$

where $A$ depends only weakly on the Manning parameter $q_0$. Taking $A = 1/2$ one finds the corresponding values for the TD ($\lambda_{\text{TD}}$) and TT ($\lambda_{\text{TT}}$) as follows:

$$\lambda_{\text{TD}} = 2.5\,\text{nm}; \qquad \lambda_{\text{TT}} = 1.1\,\text{nm}. \tag{2.7}$$

These values will be used in our calculations of the corresponding capacity and resistivity, see fig. 4.

We expect that this IC which is shielded from the cytosol by a depleted layer is an analog of a coaxial cable used in electrical engineering applications, so MTs may effectively act as nonlinear inhomogeneous transmission lines capable of propagating nonlinear dispersive ionic waves within an IC. Independent corroboration of this idea can be found in experimental assays first performed for actin filaments [26] demonstrating that an IC current along a single filament exhibits localized wave patterns similar to solitons in nonlinear electric LC transmission lines. Recently, a similar experiment was conducted on single MTs providing evidence of the amplification of input electrical signals [23]. In our model of IC currents we only consider one of the 13 parallel currents associated with a single protofilament. The elementary unit of this "nanowire" is one tubulin dimer with adjacent NPs (type-1 and type-2) and two associated TTs ($\alpha$ and $\beta$). The shape of a tubulin dimer with extended $\alpha$- and $\beta$-TTs is presented in fig. 3, including the charge distribution on its surface. At neutral $p$H values, the negative charge on each TT causes it to be extended away from the MT surface due to the electrostatic repulsion. When the negative charges of the amino acids within a TT are partly neutralized by counter-ions condensed around, it will cause TTs to contract by folding as shown in fig. 5.

As mentioned earlier, the differences in the structures of $\alpha$- and $\beta$-TTs will cause them to fold differently so that the $\beta$-TT is expected to shrink to a greater extent. In addition to these electrostatically generated conformations of TTs, their tilting oscillations due to thermal fluctuations of the environment are also present. Quantitative features of this effect will be presented in the next section. These effects are accompanied by a change in the electrostatic capacity contributed by TTs which inevitably leads

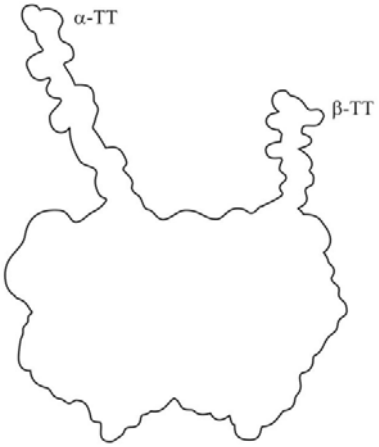


**Fig. 5.** The shape of TTs, where $\beta$-TT is shown to have shrunk due to the surrounding counter-ions, thus diminishing its electrostatic capacity.

to a slightly nonlinear overall capacity of every elementary unit of the ionic current along each filament.

## 3 The model parameters of an MT as an electric transmission line

Here, we proceed to estimate the electric parameters of an elementary unit of each MT protofilament (EUP). The essential assumption could be that an MT with a condensed IC is separated from the rest of the ions in the bulk solution by a depleted layer which plays the role of a dielectric medium located between the MT and the bulk cytosol. This IC is a conductive medium which dictates the electrical features of MTs. The depleted layer results in the IC and repelled anions playing the roles of "conductive plates" of a cylindrical capacitor. The ions injected from an appropriate cellular compartment are primarily confined to flow along an MT within its IC whose estimated thickness is $\lambda_{\rm TD} = 2.5\,{\rm nm}$.

For example, the opening of inositol (1, 4, 5) triphosphate ($IP_3$) receptors clustered at specific sites on the ER can lead to large-scale intracellular calcium waves [3,27]. By novel experimental techniques that permit the visualization of subcellular events it has become clear that $Ca^{++}$ dynamics is a highly localized process with respect to these release events and also by the channelling of these waves along cytoskeletal filaments, primarily MTs. We have earlier proposed that such $Ca^{++}$ waves could cause controlled MT depolymerisation during mitosis.

### 3.1 The capacitance of an EUP

In an earlier paper [10], a detailed Poisson-Boltzmann approach was used to evaluate the capacitance of an elementary ring of an MT which consists of 13 dimers. Here, we

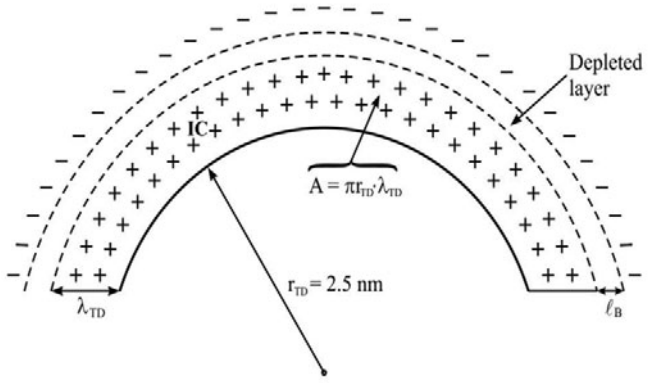


**Fig. 6.** Schematic illustration of the calculation of the MT capacitance.

adopt the same expression which reads

$$C_0 = \frac{2\pi\varepsilon_0\varepsilon l}{\ln\left(1+\frac{l_B}{R_{\rm IC}}\right)}\,, \tag{3.1}$$

where $l$ stands for the length of a polymer unit and $R_{\rm IC} = r_{\rm TD} + \lambda_{\rm TT}$ for the outer radius of an IC. The other parameters have already been introduced.

We first estimate the EUP capacitance contributed by a TD, see fig. 6. With $l_{\rm TD} = 8\,{\rm nm}$ and $R_{\rm IC} = r_{\rm TD} + \lambda_{\rm TT} = 2.5\,{\rm nm} + 2.5\,{\rm nm} = 5\,{\rm nm}$, we find for TD (including only the outer surface)

$$C_{\rm TD} = \frac{3.14\times 80\times 8.85\times 10^{-12}\times 8\times 10^{-9}}{\ln\left(1+\frac{0.67}{5}\right)}\,{\rm F} = 1.4\times 10^{-16}\,{\rm F}. \tag{3.2}$$

Analogously, we can consider an extended TT as a smaller cylinder with the radius $r_{\rm TT} = 0.5\,{\rm nm}$ and the thickness of its IC equal to $\lambda_{\rm TT} = 1\,{\rm nm}$. Its extended effective length should be $l_{\rm TT}^{\rm eff} = 4.5\,{\rm nm} - 2.5\,{\rm nm} = 2\,{\rm nm}$, meaning that its part close to the tubulin surface is already embedded in the IC accounted for in (3.2). Thus we now estimate the corresponding capacitance as:

$$C_{\rm TT} = \frac{2\times 3.14\times 80\times 8.85\times 10^{-12}\times 2\times 10^{-9}}{\ln\left(1+\frac{0.67}{1.5}\right)}\,{\rm F} = 0.26\times 10^{-16}\,{\rm F}. \tag{3.3}$$

Accounting for the fact that two TTs are present in each tubulin dimer, we finally obtain

$$2\times C_{\rm TT} = 0.52\times 10^{-16}\,{\rm F}. \tag{3.4}$$

The two capacitance values above are considered to correspond to a parallel arrangement with respect to each other, so that the total maximal capacitance of an EUP is readily estimated as

$$C_0 = C_{\rm TD} + 2\times C_{\rm TT} = 1.92\times 10^{-16}\,{\rm F}. \tag{3.5}$$

We have earlier emphasized that TTs capacitance must change with an increasing concentration of condensed

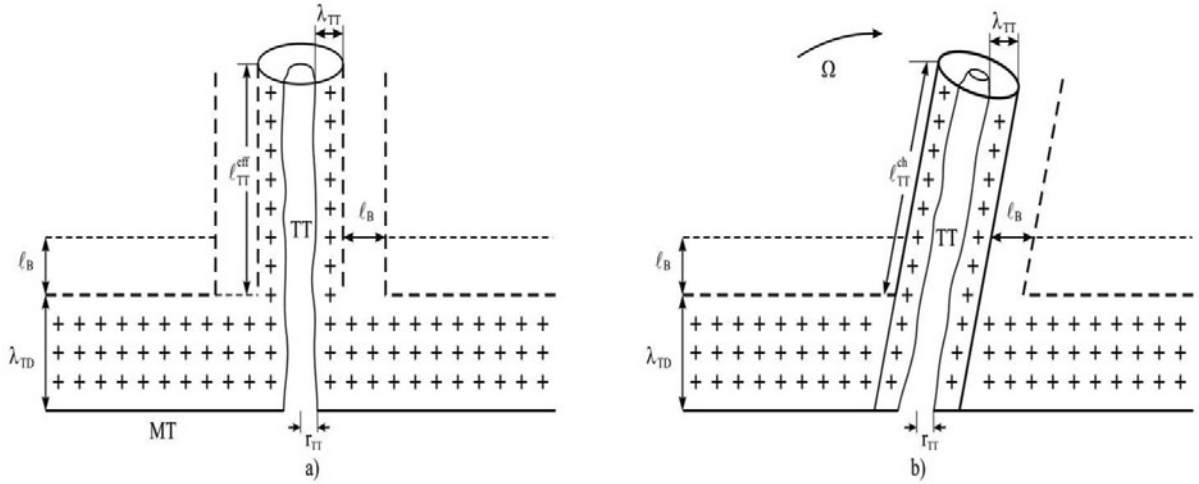


**Fig. 7.** A comparison between an extended TT (a) and a tilting TT due to oscillations (b).

cations due to the shrinking of flexible TTs. These changes are slightly different due to the different structures of $\alpha$- and $\beta$-type TTs. To include this case we introduce the reduced factor of nonlinearity as follows:

$$b_0 = \frac{b_\alpha b_\beta}{b_\alpha + b_\beta}, \tag{3.6}$$

where $b_\alpha$ and $b_\beta$ stand for the respective TTs. This implies that the charge of an EUP capacitor diminishes with an increased voltage in a nonlinear way $\Delta C_0 = C_0 b_0 v$, $b_0 v \ll 1$. Additionally, we account for the tilting movements of TTs under the combined action of thermal fluctuations [8] and a changing voltage due to an incoming ionic wave. Thus, the part of EUP capacitance contributed by TTs should also change by TTs tilt as shown in fig. 7. The change of the effective length $l_{\rm TT}^{\rm eff}$ of a TT is an additional factor affecting the capacitance $\Delta C_{\rm TT}$. We assume that this change can be adequately described by the oscillating function

$$\Delta l_{\rm TT}^{\rm eff} = l_{\rm TT}^{\rm eff} \sin[\Omega(t - t_0)] \cong l_{\rm TT}^{\rm eff} \Omega (t - t_0). \tag{3.7}$$

So that the capacitance changes linearly with a change in the effective TTs length $\Delta l_{\rm TT}^{\rm eff}$

$$\Delta C_{\rm TT} = C_0 \Gamma_0 \Omega (t - t_0), \tag{3.8}$$

where the frequency $\Omega$ is much lower than the inverse charging time of the EUP capacitor due to the strong viscous damping of the TT tilt, thus justifying the linearization of the above sine function in eq. (3.7). In some sense, this effect is similar in character to the thermal ratchet mechanism combined with an asymmetric ionic potential. Including the two aspects of TTs dynamics described above, the charge of EUP can be expressed as follows

$$Q = C_0[1 - \Gamma_0 \Omega (t - t_0) - b_0 v]v, \tag{3.9}$$

where $\Gamma_0$ is a dimensionless parameter.

In the earlier simplified version of the model of ionic currents along MT [10], a proof was given that the order of magnitude of magnetic inductance is so small that its role in these transmission lines can be safely ignored. We accept this statement in the present paper.

### 3.2 The resistance of an EUP

Regarding the Ohmic resistance, if we ignore ionic current leaks through the depleted layer, the dominant current flows in parallel with the MT axis charging EUP capacitors and partly leaking through NPs. The resistance attributed to this kind of ionic flow can be estimated on the basis of experimental evidence provided by the electro-orientation method performed on MTs *in vitro* [25]. Taking the reported measured value of MT ionic conductivity as

$$\sigma = (0.15 \pm 0.01)\,{\rm S\,m^{-1}}, \tag{3.10}$$

and adopting a simplifying assumption that the resistivity within an IC patch beyond an EUP is homogeneous, the resistance of an EUP with the length $l = 8\,{\rm nm}$ and the cross-sectional area $A = \pi r_{\rm DT} \lambda_{\rm DT} = 3.14 \times 2.5\,{\rm nm} \times 2.5\,{\rm nm} = 19.625\,{\rm nm^2}$, see fig. 6, is estimated as $R_0 = \frac{1}{\sigma}\frac{l}{A} = 2.7 \times 10^9\,\Omega$. This is obviously an extremely high value of resistance which is most likely an over-estimate.

We therefore prefer the computed resistance shown in table 3 of ref. [8], referred to as the outer sheath-outer sheath resistance for complete 13 protofilaments, namely $R_{13} = 4.75 \times 10^6\,\Omega$. The resistance for our EUP will be 13 times greater, *i.e.*

$$R_0 = 6.2 \times 10^7\,\Omega. \tag{3.11}$$

This value appears to be more consistent with the resistance of two NPs which follows from eq. (3.12).

Finally, we could include the conductance of both NPs to account for the leakage of IC cations into the lumen area. Thus we have

$$G_0 = \sigma_1 + \sigma_2 = (2.93 + 7.8)\,{\rm nS} = 10.7\,{\rm nS}; \quad \frac{1}{G_0} = 9.3 \times 10^7. \tag{3.12}$$

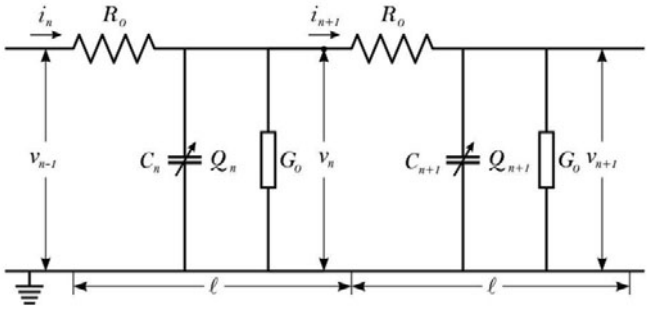


**Fig. 8.** An effective circuit diagram for the $n$-th ER with characteristic elements for Kirchhoff's laws.

It is expected that NPs exert greater resistance than the volume of IC around EUP. The above features of EUP electric parameters will lead to biophysical implications of our model. The next section develops the underlying equations governing the ionic flows along MTs.

## 4 The generalized model of an MT as a nonlinear transmission line

We now construct a simple periodic electric circuit simulating one protofilament of an MT. It consists of a long ladder network composed of a lumped section equal to identical EUPs as represented in fig. 8.

The longitudinal ionic current is represented by the series of resistors with Ohmic resistance $R_0$ for one EUP, as represented in (3.11). The nonlinear capacity with the charge $Q_n$ for the $n$-th site of the ladder network is in parallel with the total conductance $G_0$ of the two TTs expressed by eq. (3.12). This is true if the bulk cytosol and MT lumen are considered to be grounded. This permits the application of Kirchhoff's law as

$$i_n - i_{n+1} = \frac{\partial Q_n}{\partial t} + G_0 v_n, \tag{4.1}$$

$$v_{n-1} - v_n = R_0 i_n. \tag{4.2}$$

Using eq. (3.9) and taking the time derivative results in a nonlinear form of the governing equation since

$$\frac{\partial Q}{\partial t} = C_0 \frac{\partial v_n}{\partial t} - C_0 \Gamma_0 \Omega v_n - C_0 \Gamma_0 \Omega (t - t_0) \frac{\partial v_n}{\partial t} - 2 b_0 C_0 v_n \frac{\partial v_v}{\partial t}. \tag{4.3}$$

Inserting eq. (4.3) into eq. (4.1) we arrive at the explicit system of equations describing the ionic current within IC, and an accompanying voltage

$$i_n - i_{n+1} = C_0 \frac{\partial v_n}{\partial t} - C_0 \Gamma_0 \Omega v_n - C_0 \Gamma_0 \Omega (t - t_0) \frac{\partial v_n}{\partial t} - 2 b_0 C_0 v_n \frac{\partial v_v}{\partial t} + G_0 v_n, \tag{4.4}$$

$$v_{n-1} - v_n = R_0 i_n. \tag{4.5}$$

The next step is to establish the auxiliary function $u(x,t)$ unifying the voltage and its accompanying ionic current as follows:

$$u_n = Z^{1/2} i_n = Z^{-1/2} v_n, \tag{4.6}$$

where the characteristic impedance of EUP is defined in the usual way as

$$Z = \frac{1}{\omega C_0}. \tag{4.7}$$

Since the discrete voltage $v_n$ as well as the associated current $i_n$ change gradually from an EUP to its neighbors, we can safely justify the expansion of $u_n$ in a continuum approximation using a Taylor series with respect to a small spatial parameter $l$ ($l = 8\,\mathrm{nm}$ is the length of an EUP). Then using the travelling-wave form of the function $u(x,t)$ with dimensionless space and time variables $(\xi, \tau)$, we eventually get the following inhomogeneous nonlinear partial differential equation (for details see appendix B):

$$\left(\frac{ZC_0 s}{T_0} - 2\right) \frac{\partial u}{\partial \tau} + \frac{1}{3} \frac{\partial^3 u}{\partial \xi^3} + ZC_0 \Gamma_0 \Omega (\xi - \xi_0) \frac{\partial u}{\partial \xi} + 2 \frac{Z^{3/2} b_0 C_0 s}{T_0} u \frac{\partial u}{\partial \xi} + (ZG_0 + Z^{-1} R_0 - ZC_0 \Gamma_0 \Omega) u = 0. \tag{4.8}$$

Here, the characteristic charging (discharging) time of an EUP capacitor $C_0$ through the resistance $R_0$, $T_0 = R_0 C_0$, on the basis of eqs. (3.5) and (3.11) yields the value

$$T_0 = 6.2 \times 10^7\,\Omega \times 1.92 \times 10^{-16}\,\mathrm{F} = 1.2 \times 10^{-8}\,\mathrm{s}. \tag{4.9}$$

The characteristic propagation velocity of the ionic wave is defined as follows:

$$v_0 = \frac{8 \times 10^{-9}\,\mathrm{m}}{1.2 \times 10^{-8}\,\mathrm{s}} = 0.67 \frac{\mathrm{m}}{\mathrm{s}}. \tag{4.10}$$

The dimensionless speed, space and time variables are chosen to be, respectively,

$$s = \frac{v}{v_0} \leq 1; \quad \xi = \frac{x}{l} - \tau; \quad \tau = s \frac{t}{T_0}. \tag{4.11}$$

Imposing that the condition

$$\frac{ZC_0 s}{T_0} > 2 \tag{4.12}$$

holds, we then estimate the characteristic impedance of EUP as

$$Z > \frac{2R_0}{s} \quad \text{or} \quad Z > 1.24 \times 10^8\,\Omega \quad \text{for} \quad s = 1. \tag{4.13}$$

For $s = 1$ one obtains the cutoff frequency

$$\omega_{\max} = 4.3 \times 10^7\,\mathrm{s}^{-1} \qquad \text{or} \qquad \nu_{\max} = 6.8 \times 10^6\,\mathrm{Hz}. \tag{4.14}$$

This indicates that the characteristic frequency matches the order of magnitude of frequency $\Omega$ which describes

$$W(\xi,\tau)=\frac{u_0}{\cosh^2\left\{\left[\frac{\alpha u_0}{4\beta}\exp(-2\gamma_0\tau)\right]^{1/2}\left[\xi-\xi_0\left(1-\exp(\gamma_0\tau)\right)+\frac{\alpha u_0}{3\beta}\left(1-\exp(3\gamma_0\tau)\right)\exp(-2\gamma_0\tau)\right]\right\}}, \tag{4.28}$$

$$u(\xi,\tau)=\frac{u_0\exp(-2\gamma_0\tau)}{\cosh^2\left\{\left[\frac{\alpha u_0}{4\beta}\exp(-2\gamma_0\tau)\right]^{1/2}\left[\xi-\xi_0\left(1-\exp(\gamma_0\tau)\right)+\frac{\alpha u_0}{3\beta}\left(1-\exp(3\gamma_0\tau)\right)\exp(-2\gamma_0\tau)\right]\right\}}. \tag{4.29}$$

the TTs oscillations. We now establish the compact form of eq. (4.8) as

$$\frac{\partial u}{\partial\tau}+\beta\frac{\partial^3 u}{\partial\xi^3}+\alpha u\frac{\partial u}{\partial\xi}+\gamma(\xi)\frac{\partial u}{\partial\xi}+\delta u=0, \tag{4.15}$$

where the abbreviations were introduced as follows:

$$\left.\begin{aligned}
&\alpha=\frac{2Z^{3/2}b_0C_0s}{T_0\left(\frac{ZC_0s}{T_0}-2\right)};\quad \beta=\frac{1}{3\left(\frac{ZC_0s}{T_0}-2\right)};\\
&\delta=\frac{ZG_0+Z^{-1}R_0-ZC_0\Gamma_0\Omega}{\left(\frac{ZC_0s}{T_0}-2\right)};\\
&\gamma(\xi)=\frac{ZC_0\Gamma_0\Omega(\xi-\xi_0)}{\left(\frac{ZC_0s}{T_0}-2\right)}=\gamma_0(\xi-\xi_0);\\
&\gamma_0=\frac{ZC_0\Gamma_0\Omega}{\left(\frac{ZC_0s}{T_0}-2\right)}.
\end{aligned}\right\} \tag{4.16}$$

We can further perform the following transformation of space-time variables $(\xi,\tau)\to(\rho,\theta)$:

$$\left.\begin{aligned}
&\rho(\xi,\tau)=(\xi-\xi_0)\exp(-\gamma_0\tau),\\
&\theta(\tau)=-\frac{1}{3\gamma_0}\exp(-3\gamma_0\tau),\\
&u(\xi,\tau)=W(\rho,\theta)\exp(-2\gamma_0\tau),
\end{aligned}\right\} \tag{4.17}$$

so that eq. (4.15) takes the simplified form

$$\frac{\partial W}{\partial\theta}+\alpha W\frac{\partial W}{\partial\rho}+\beta\frac{\partial^3 W}{\partial\rho^3}+\frac{\kappa}{\theta}W=0, \tag{4.18}$$

where the new parameter $\kappa$ reads

$$\kappa=\frac{2}{3}-\frac{\delta}{3\gamma_0}. \tag{4.19}$$

If we assume that the Ohmic losses in this circuit are balanced by the "thermal ratchet" action of TTs, then the last term in eq. (4.15) vanishes so that

$$\frac{2}{3}-\frac{\delta}{3\gamma_0}=0;\quad \delta=2\gamma_0. \tag{4.20}$$

This gives the following condition:

$$ZG_0+Z^{-1}R_0=3ZC_0\Gamma_0\Omega;\quad Z=\frac{1}{\omega C_0}. \tag{4.21}$$

Furthermore, if we impose the simple condition

$$\left(\frac{ZC_0s}{T_0}-2\right)=1,\quad \text{with}\quad s=1,$$

we then obtain the values

$$Z=1.87\times10^8\,\Omega\quad\text{and}\quad\omega=2.7\times10^7\,\mathrm{s}^{-1}. \tag{4.22}$$

Subsequently, equating $\omega=\Omega=2.7\times10^7\,\mathrm{s}^{-1}$ we estimate the parameter $\Gamma_0$ directly from eq. (4.21) as

$$\Gamma_0=\frac{G_0}{3C_0\omega}+\frac{C_0R_0\omega}{3}=0.07+0.11=0.18. \tag{4.23}$$

Eventually, the spatial inhomogenity parameter is found to be

$$\Gamma_0\,\Omega=4.8\times10^6\,\mathrm{s}^{-1}, \tag{4.24}$$

which is one order of magnitude smaller than the inverse characteristic time $T_0^{-1}=1.83\times10^7\,\mathrm{s}^{-1}$, thus justifying eq. (3.7). In such a case ($\kappa=0$), eq. (4.18) reduces to the modified nonlinear KdV equation with spatial inhomogeneity which exhibits a single bell-shaped soliton solution subjected to the distortion due to the Ohmic dissipation. In reality, the condition in eq. (4.20) seems to be reasonably met. Otherwise, if $\kappa=1$ or $\kappa=2$, eq. (4.18) reduces to a nonlinear spherical (cylindrical) KdV equation which has already been derived in the context of ionic-acoustic plasma waves [28,29]. In general, by introducing the new transformation [30]

$$F=W\exp\left(\sigma\int\frac{\mathrm{d}\theta}{\theta}\right), \tag{4.25}$$

and substituting to eq. (4.18) we obtain

$$\frac{\partial F}{\partial\theta}=\Lambda(\theta)\cdot F\frac{\partial F}{\partial\xi}+\beta\frac{\partial^3 F}{\partial\xi^3}=0, \tag{4.26}$$

where the new function $\Lambda(\theta)$ reads

$$\Lambda(\theta)=\alpha\exp\left(-\alpha\int\frac{\mathrm{d}\theta}{\theta}\right). \tag{4.27}$$

The solution of (4.18) with $\kappa=0$ is expressed as

*see equation* (4.28) *above*

so that the function $u(\xi,\tau)$ has the form

*see equation* (4.29) *above*

If we use the set of estimated and chosen parameters in eqs. (3.5), (3.11), (3.12), (4.21) and (4.24), we readily see that all dimensionless parameters (4.16) lie between zero and one ($\beta = 0.33$, $\gamma_0 = 0.17$, $\delta = 0.34$) staying within the same order of magnitude. This suggests that we should inspect numerically the behavior of the solution of eq. (4.29) when the parameters $\alpha$, $\beta$, $\gamma_0$, $\xi_0$ take slightly different values which is done next.

Analyzing the set of plots in fig. 9 we can see the competition between nonlinearity $\alpha$ and the dispersion $\beta$, as well as the role of inhomogenity $\gamma_0$. In the case represented in fig. 9b we have balanced all parameters. The soliton solution preserves its width but its amplitude decays rather rapidly so that over the length of about $500l$ it becomes negligible. The above view shows the deceleration of the soliton solution along its path. Figure 9c shows the case with increased nonlinearity ($\alpha = 0.5$). It is remarkable that it exhibits not only a higher localization but also a slower decay of its amplitude. The advantage of this case lies in the fact that the velocity of the soliton solution decreases very slightly. We estimate its average velocity as follows:

$$\Delta x \approx 400l = 400 \times 8\,\mathrm{nm} = 3.2\,\mu\mathrm{m},$$
$$\Delta t = 1000T_0 = 10^3 \times 1.2 \times 10^{-8}\,\mathrm{s} = 1.2 \times 10^{-5}\,\mathrm{s},$$
$$v = \frac{\Delta x}{\Delta t} = 0.26\frac{\mathrm{m}}{\mathrm{s}}\,.$$

The range of this soliton is $3.2\,\mu$m which is of the order of the cell's diameter. Therefore, it appears that the ionic pulse with such parameter values could be efficiently transferred within the cell.

## 5 Conclusions and discussion

In this paper we have developed a nonlinear model of ionic currents along MTs in the context of the polyelectrolyte character of these cytoskeletal filaments. We have taken into account the role of two aspects of this cylindrical biopolymer, its NPs and very sensitive TTs. Both of them are responsible for the nonlinear character of the overall electrical capacitance of MTs. Segmenting an MT into identical EUPs and estimating the values of corresponding electrical parameters, we were able to establish the difference equations of lumped EUP sections, eq. (4.1) and eq. (4.2). On the basis of a gradual change of voltage along MT protofilaments we imposed a continuum approximation limit leading to the nonlinear KdV type equation in (4.15) with dissipative and inhomogeneity terms, $\delta$ and $\gamma(\xi)$, eq. (4.16). This sort of equation was derived earlier within non-uniform plasma applications where ion acoustic solitons were identified, both in the cases of cylindrical and spherical geometry.

Our solution, eq. (4.29), was analysed numerically for the set of parameters in fig. 9. It is apparent that the solitonic wave loses its energy due to Ohmic resistance but it preserves the stable localised form. In the case presented in fig. 9c with an increased nonlinearity parameter, the solitonic pulse exhibits greater robustness and it progresses with an almost constant velocity and only a slight decay of its initial amplitude. This demonstrates the role of flexible TTs which could be of decisive importance for the stable localized character of ionic pulses along MTs. Interestingly, TTs are the structural elements of tubulin with the greatest diversity across cells and biological species which could be of functional significance. Moreover, it was earlier shown that MTs posses ferroelectric properties creating an intrinsic electric field [31]. It is expected that this intrinsic electric field within an MT provides the necessary electrostatic energy which may compensate for the losses due to viscosity and thus enable the near lossles propagation of solitonic pulses over long distances along MTs.

We expect that this type of localized ionic waves could play a fundamental role in many cellular processes. First the process of cell division, in the context described by Hepler [3,4], needs the synchronized depolymerisation of MTs. This can be caused by the localized $Ca^{++}$ waves described by our model which could reach MT plus ends and trigger the onset of massive detachment of TDs from MT tips [32]. If this process were to be based on pure diffusion of $Ca^{++}$ ions through the bulk cytosol, the resulting depolymerisation would be prone to frequent mistakes making this process very unreliable which known not to be the case.

In a very interesting paper Duke [33] explained that in hair bundles (kinocilium) in the inner ear consisting of MT doublets, the myosin motor-driven oscillation are controlled by $Ca^{++}$ ions directed from ion channels along MTs. These ions cause a fraction of myosin motors to detach and thus tune the oscillations of kinocilium as reaction to a corresponding acoustic signal. This mechanism can also be seen in the context of localized $Ca^{++}$ waves described in the present paper.

Finally, the experimental work of Priel *et al.* [23] demonstrated that the electrical signal amplification resulting from the presence of MTs can be directly attributed to nonlinear ionic currents guided by MTs in close similarity to the framework developed by our present model. In fact, these measurements inspired the authors to consider the role MTs can play as bio-transistors taking part in cognitive processes which is another interesting application of nonlinear ionic conductance of MTs.

This research was supported by funds from Serbian Ministry of Science, Grants: III43008 and 171009. Jack A. Tuszynski acknowledges support for his research from NSERC (Canada).

## Appendix A. Glossary

ER: endoplasmic reticulum
EUP: elementary unit of protofilament
IC: ionic cloud
KdV: Korteveg de Vries
MT: microtubule
NP: nano-pore
TD: tubulin dimer
TT: tubulin tail

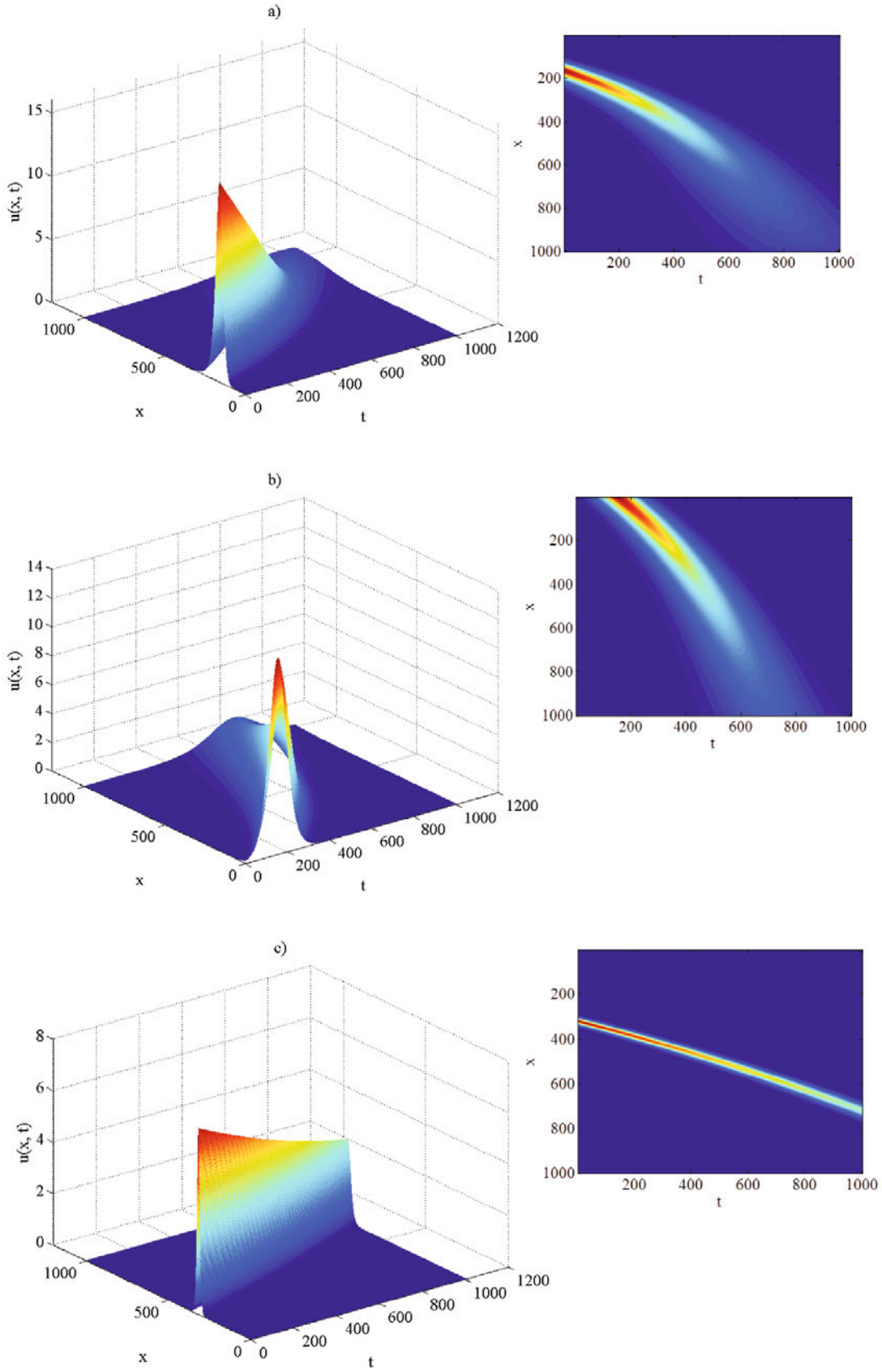


**Fig. 9.** Numerical solutions of $u(\xi, \tau)$ for: a) $\alpha = 0.2$; $\gamma_0 = 0.17$; $\beta = 0.33$; $\xi_0 = 0.1$. b) $\alpha = 0.1$; $\gamma_0 = 0.1$; $\beta = 0.1$; $\xi_0 = 0.1$. c) $\alpha = 0.5$; $\gamma_0 = 0.1$; $\beta = 0.1$; $\xi_0 = 0.1$.

## Appendix B.

Using a Taylor series as follows:

$$u_{n\pm1} = u \pm l\frac{\partial u}{\partial x} + \frac{l^2}{2!}\frac{\partial^2 u}{\partial x^2} \pm \frac{l^3}{3!}\frac{\partial^3 u}{\partial x^3} + \frac{l^4}{4!}\frac{\partial^4 u}{\partial x^4} \pm \frac{l^5}{5!}\frac{\partial^5 u}{\partial x^5} + \ldots, \tag{B.1}$$

and applying on eqs. (4.4) and (4.5) this system now reads

$$-\frac{\partial u}{\partial x} - \frac{l}{2}\frac{\partial^2 u}{\partial x^2} - \frac{l^2}{6}\frac{\partial^3 u}{\partial x^3} - \frac{l^3}{24}\frac{\partial^4 u}{\partial x^4} - \frac{l^4}{120}\frac{\partial^5 u}{\partial x^5} - \frac{ZG_0}{l}u - \frac{ZC_0}{l}\frac{\partial u}{\partial t} + \frac{ZC_0\Gamma_0\Omega}{l}u + \frac{ZC_0\Gamma_0\Omega}{l}(t-t_0)\frac{\partial u}{\partial t} + 2\frac{Z^{3/2}b_0C_0}{l}u\frac{\partial u}{\partial t} = 0, \tag{B.2}$$

$$-\frac{\partial u}{\partial x} + \frac{l}{2}\frac{\partial^2 u}{\partial x^2} - \frac{l^2}{6}\frac{\partial^3 u}{\partial x^3} + \frac{l^3}{24}\frac{\partial^4 u}{\partial x^4} - \frac{l^4}{120}\frac{\partial^5 u}{\partial x^5} - \frac{Z^{-1}R_0}{l}u = 0. \tag{B.3}$$

Adding up the last two equations and retaining the terms up to the order of the third derivative, due to smallness of $l^4$, we obtain

$$-2\frac{\partial u}{\partial x} - \frac{l^2}{3}\frac{\partial^3 u}{\partial x^3} - \frac{ZC_0}{l}\frac{\partial u}{\partial t} + \frac{ZC_0\Gamma_0\Omega}{l}(t-t_0)\frac{\partial u}{\partial t} + 2\frac{Z^{3/2}b_0C_0}{l}u\frac{\partial u}{\partial t} - \frac{1}{l}(ZG_0 + Z^{-1}R_0 - ZC_0\Gamma_0\Omega)u = 0. \tag{B.4}$$

Then the standard travelling wave with speed $v$, for the unified function $u(x,t)$, can be employed as follows:

$$\left.\begin{aligned} &u(x,t) = u\left(\frac{x}{l} - v\frac{t}{l}\right) = u\left(\frac{x}{l} - \frac{v}{v_0}v_0\frac{t}{l}\right) = \\ &u\left(\frac{x}{l} - s\frac{t}{T_0}\right) = u(\xi), \\ &\xi = \frac{x}{l} - \tau; \quad \tau = s\frac{t}{T_0}; \quad v_0 = \frac{l}{T_0}; \quad s = \frac{v}{v_0}. \end{aligned}\right\} \tag{B.5}$$

In that respect, the set of the following transformations holds:

$$\frac{\partial u}{\partial x} = \frac{1}{l}\frac{\partial u}{\partial \xi}; \quad \frac{\partial^3 u}{\partial x^3} = \frac{1}{l^3}\frac{\partial^3 u}{\partial \xi^3}; \quad \frac{\partial u}{\partial t} = \frac{s}{T_0}\frac{\partial u}{\partial \tau} = -\frac{s}{T_0}\frac{\partial u}{\partial \xi}. \tag{B.6}$$

Using the transformations given by eqs. (B.5) and (B.6) and retaining the first derivatives of $\tau$ and going over to space derivatives of $\xi$ in the inhomogeneous (fourth) term and nonlinear (fifth) term of eq. (B.4), we readily find

$$\left(\frac{ZC_0 s}{T_0} - 2\right)\frac{\partial u}{\partial \tau} + \frac{1}{3}\frac{\partial^3 u}{\partial \xi^3} + ZC_0\Gamma_0\Omega(\xi - \xi_0)\frac{\partial u}{\partial \xi} + 2\frac{Z^{3/2}b_0C_0 s}{T_0}u\frac{\partial u}{\partial \xi} + \left(ZG_0 + Z^{-1}R_0 - ZC_0\Gamma_0\Omega\right)u = 0. \tag{B.7}$$

## References


1. L.A. Amos, Trends Cell Biol. **5**, 48 (1995).
2. G. Matsumoto, M. Ishikawa, A. Tasaki, H. Murofushi, H. Sakai, J. Membr. Biol. **77**, 77 (1989).
3. P.K. Hepler, Plant Cell **17**, 2142 (2005).
4. D.H. Chang, P. Wadsworth, P.K. Hepler, J. Cell Sci. **102**, 79 (1992).
5. L. Matsson, J. Biol. Phys. **31**, 303 (2005).
6. L. Matsson, J. Phys.: Condens. Matter **21**, 502101 (2009).
7. E. Nogales, H.W. Wang, Curr. Opin. Cell Biol. **18**, 179 (2006).
8. H. Freedman, V. Rezania, A. Priel, E. Carpenter, S.Y. Noskov, J.A. Tuszynski, Phys. Rev. E **81**, 051912 (2010).
9. J.F. Diaz, I. Barasoain, J.M. Andren, J. Biol. Chem. **278**, 8407 (2003).
10. M.V. Satarić, D.I. Ilić, N. Ralević, J.A. Tuszynski, Eur. Biophys. J. **38**, 637 (2009).
11. M.V. Satarić, D. Sekulić, M. Živanov, J. Comput. Theor. Nanosci. **7**, 2281 (2010).
12. Z.S. Siwy, M.R. Powell, A. Petrov, E. Kalman, C. Trantmann, R.S. Eisenberg., Nano Lett. **6**, 1729 (2006).
13. W. Im, B. Roux, J. Mol. Biol. **322**, 851 (2002).
14. L. Serrano, J. de la Torre, R.B. Maccioni, Y. Avila, Biochemistry **23**, 4675 (1984).
15. M.V. Satarić, J.A. Tuszynski, Phys. Rev. E **67**, 011901 (2003).
16. N.A. Baker, D. Sept, S. Joseph, M.J. Holst, J.A. McCammon, Proc. Natl. Acad. Sci. U.S.A. **98**, 10037 (2001).
17. J.A. Tuszynski, J.A. Brown, E. Crowford, E.J. Carpenter, M.L.A. Nip, J.M. Dixon, M.V. Satarić, Math. Comput. Modell. **41**, 1055 (2005).
18. G.S. Manning, Rev. Biophys. **2**, 179 (1978).
19. J.A. Tuszynski, A. Priel, J.A. Brown, H.F. Cantiello, J.M. Dixon, *Nano and Molecular Electronics Handbook, Electronic and Ionic Conductivities of Microtubules and Actin Filaments: Their Consequences for Cell Signaling and Applications to Bioelectronics* (Taylor and Francis, London, 2007).
20. A. Priel, J.A. Tuszynski, H. Cantielo, *Molecular Biology of the Cell, Ionic Waves Propagation Along the Dendritic Cytoskeleton as a Signaling Mechanism* (Elsevier, 2006).
21. A. Priel, J.A. Tuszynski, EPL **83**, 68004 (2008).
22. J.A. Tuszynski, S. Portet, J.M. Dixon, C. Luxford, H.F. Cantiello, Biophys. J. **86**, 1890 (2004).
23. A. Priel, A.J. Ramos, J.A. Tuszynski, H.F. Contiello, Biophys. J. **90**, 4639 (2006).
24. B. O'Shanghnessy, Q. Yang, Phys. Rev. Lett. **94**, 048302 (2005).
25. I. Minoura, E. Muto, Biophys. J. **90**, 3739 (2006).
26. C. Lin, H.F. Cantiello, Biophys. J. **65**, 1371 (1993).
27. K. Wang, W.J. Rappel, H. Levine, Phys. Biol. **1**, 27 (2004).
28. S. Maxon, J. Viecelli, Phys. Rev. Lett. **32**, 4 (1974).
29. S. Maxon, J. Viecelli, Phys. Fluids **17**, 1614 (1974).
30. T. Yagy, J. Phys. Soc. Jpn. **50**, 2737 (1981).
31. J.A. Tuszynski, S. Hameroff, M.V. Satarić, B. Tripisova, M.L.A. Nip, J. Theor. Biol. **174**, 371 (1995).
32. L.J. Gagliardi, J. Electrostat. **54**, 219 (2002).
33. T. Duke, J. Phys.: Condens. Matter **15**, S1747 (2003).